BIOCHEMISTRY
including biophysical chemistry & molecular biology

Article

pubs.acs.org/biochemistry

Kinetic Mechanism of Indole-3-glycerol Phosphate Synthase

Sandra Schlee,*[,†] Susanne Dietrich,[†] Tomasz Kurćon,[‡,§] Pamela Delaney,[‡] Nina M. Goodey,*[,‡] and Reinhard Sterner[†]

[†]Institute of Biophysics and Physical Biochemistry, University of Regensburg, Universitätsstrasse 31, D-93053 Regensburg, Germany

[‡]Department of Chemistry and Biochemistry, Montclair State University, RI 346, 1 Normal Avenue, Montclair, New Jersey 07043, United States

[§]Department of Chemistry, New York University, New York, New York 10003, United States

Supporting Information

ABSTRACT: The $(\beta\alpha)_8$-barrel enzyme indole-3-glycerol phosphate synthase (IGPS) catalyzes the multistep transformation of 1-(*o*-carboxyphenylamino)-1-deoxyribulose 5-phosphate (CdRP) into indole-3-glycerol phosphate (IGP) in tryptophan biosynthesis. Mutagenesis data and crystal structure analysis of IGPS from *Sulfolobus solfataricus* (sIGPS) allowed for the formulation of a plausible chemical mechanism of the reaction, and molecular dynamics simulations suggested that flexibility of active site loops might be important for catalysis. Here we developed a method that uses extrinsic fluorophores attached to active site loops to connect the kinetic mechanism of sIGPS to structure and conformational motions. Specifically, we elucidated the kinetic mechanism of sIGPS and correlated individual steps in the mechanism to conformational motions of flexible loops. Pre-steady-state kinetic measurements of CdRP to IGP conversion monitoring changes in intrinsic tryptophan and IGP fluorescence provided a minimal three-step kinetic model in which fast substrate binding and chemical transformation are followed by slow product release. The role of sIGPS loop conformational motion during substrate binding and catalysis was examined via variants that were covalently labeled with fluorescent dyes at the N-terminal extension of the enzyme and mobile active site loop $\beta1\alpha1$. Analysis of kinetic data monitoring dye fluorescence revealed a conformational change that follows substrate binding, suggesting an induced-fit-type binding mechanism for the substrate CdRP. Global fitting of all kinetic results obtained with wild-type sIGPS and the labeled variants was best accommodated by a four-step kinetic model. In this model, both the binding of CdRP and its on-enzyme conversion to IGP are accompanied by conformational transitions. The liberation of the product from the active site is the rate-limiting step of the overall reaction. Our results confirm the importance of flexible active loops for substrate binding and catalysis by sIGPS.

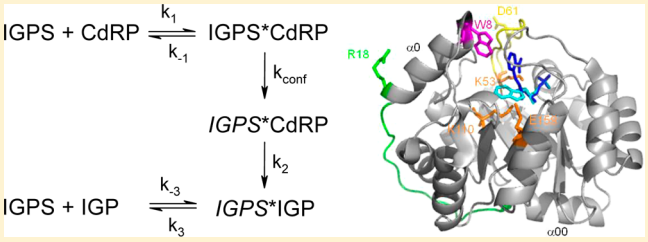

Indole-3-glycerol phosphate synthase (IGPS) catalyzes the fifth reaction in the biosynthesis of tryptophan, whereby the enzyme facilitates a ring closure reaction of the substrate 1-(*o*-carboxyphenylamino)-1-deoxyribulose 5-phosphate (CdRP) to the product indole-3-glycerol phosphate (IGP) (Figure 1A). The chemical reaction consists of a sequence of condensation, decarboxylation, and dehydration and is irreversible, because of both the formation of the pyrrole ring of the indole and the release of CO_2.[1] The crystal structures of apo forms of the bifunctional enzyme IGPS/phosphoribosyl anthranilate isomerase from *Escherichia coli* (eIGPS:ePRAI)[2,3] as well as those of the monofunctional IGPS from the hyperthermophiles *Sulfolobus solfataricus* (sIGPS)[4,5] and *Thermotoga maritima*,[6] which optimally grow at ~80 °C, have been determined at 2 Å resolution. IGPS has the ubiquitous $(\beta\alpha)_8$-barrel fold, with an N-terminal extension of ~45 residues. In sIGPS, the latter comprises the additional $\alpha0$ and $\alpha00$ helices that are connected by the $\alpha0\alpha00$ loop (Figure 1B).

The highly conserved residues Lys53, Lys110, Glu159, and Asn180 (sIGPS numbering) were identified as being essential for catalysis by mutational analyses of eIGPS.[7,8] These findings were confirmed by crystal structures of sIGPS with bound substrate CdRP, substrate analogue rCdRP, and product IGP.[9] The chemical mechanism deduced from these data is based on general acid−base catalysis, whereby the charged ε-amino group of Lys110 acts as the general acid and the carboxylate group of Glu159 (or Glu210[10]) acts as the general base. The structures of sIGPS with substrate CdRP and product IGP illustrate that two distinct but adjacent hydrophobic pockets are involved in binding of the substrate and product (Figure 1B). Certain hydrophobic side chains contact the benzene ring of (r)CdRP, others the benzene ring of IGP, and some both. Importantly, the substrate CdRP is bound in an unproductive mode in the crystal structure, because the distance between the two carbon atoms, C1 and C2′, that are to be joined is too large for the formation of a covalent bond.[9] Both observations

Received: October 2, 2012
Revised: December 10, 2012
Published: December 10, 2012

   dx.doi.org/10.1021/bi301342j | *Biochemistry* 2013, 52, 132−142

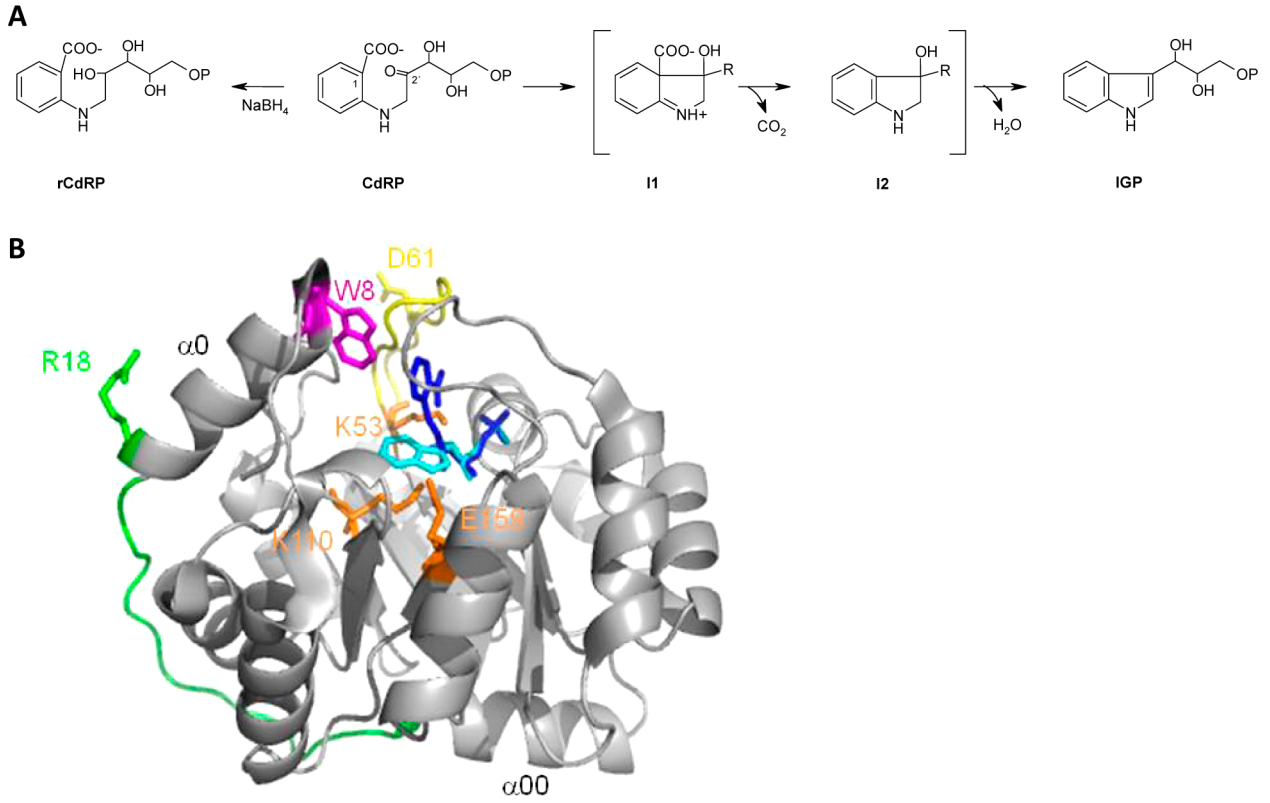

Figure 1. Reaction catalyzed by IGPS and crystal structure of sIGPS. (A) The enzyme facilitates a ring closure reaction of the substrate CdRP to the product IGP. The chemical reaction consists of a sequence of condensation, decarboxylation, and dehydration. It comprises the two intermediates, I1 and I2, and is irreversible. Chemical reduction of CdRP by borohydride produces the substrate analogue rCdRP. (B) Crystal structure of sIGPS with substrate CdRP (blue) [Protein Data Bank (PDB) entry 1LBL] and product IGP (cyan) (PDB entry 1A53). The substrate and product bind to adjacent but distinct hydrophobic pockets. Two variants of sIGPS were generated for fluorescence labeling, during which residues either in the N-terminal extension [R18 at the boundary of α-helix α0 to loop α0α00 (green)] or within a flexible loop at the catalytic face [D61 on loop β1α1 (yellow)] were replaced with cysteines. The single tryptophan residue, W8, which was used to monitor intrinsic fluorescence, is colored magenta, and residues essential for catalysis (K53, K110, and E159) are colored orange.

indicate that conformational rearrangements at the active site might take place during the reaction cycle.

In accordance with this hypothesis, experimental and computational data suggest that residues from the two flexible loops, β1α1 (comprising residues Lys53−Asp65) and α0α00 (comprising residues Arg18−Ser32), are involved in the reaction. The Lys53Ser replacement in loop β1α1 decreases catalytic turnover number k_{cat} by 20-fold and increases Michaelis constant K_M^{CdRP} by 2000-fold.[7,9] The comparison of the crystal structures with bound (r)CdRP and IGP indicates that the positively charged side chain of Lys53, which forms electrostatic interactions with both the carboxylate and the C3′ hydroxyl groups of CdRP, guides the substrate from one hydrophobic pocket to the other.[7,9] Moreover, molecular dynamics (MD) simulations have suggested that the electrostatic interactions of the side chain of Lys53 with CdRP are weakened at the high physiological temperatures of sIGPS, leading to a reorientation of C1 and C2′ that favors bond formation.[10,11] MD simulations also indicated that the temperature-induced increased mobility of Lys53 alters its interaction with the general acid Lys110. As a consequence, the ε-amino group of Lys110 moves closer to the C2′ oxygen of the substrate, facilitating its protonation.[12] Moreover, the analysis of three different crystal forms of sIGPS showed large deviations in the Cα positions between Pro57 and Glu63 and suggested the population of at least two distinct low-energy conformations for loop β1α1.[6] A sIGPS variant lacking the 26 N-terminal residues, including helix α0 and the first half of loop α0α00, displayed an unaltered k_{cat} value but a 3000-fold increased K_M^{CdRP} value in comparison to those of wild-type sIGPS.[13] These findings are explained by the fact that Trp8 from helix α0 is part of the anthranilate-binding pocket[9] and suggest that adjacent flexible loop α0α00 might undergo a conformational motion upon substrate binding.

The purpose of this study was the elucidation of the kinetic reaction mechanism of sIGPS and its correlation with conformational motions of loops β1α1 and α0α00. For this purpose, we performed steady-state and pre-steady-state kinetic analyses of CdRP to IGP conversion by wild-type sIGPS (sIGPS-wt). Global fitting of the combined data with a minimal three-step model provided the individual rate constants for substrate binding, chemistry, and product release. To integrate kinetic data with conformational motions during substrate binding and catalysis, we generated variants that were covalently labeled with fluorescent dyes at two active site loops. Analysis of single-turnover kinetics of the labeled variants detected by both product accumulation and dye fluorescence revealed conformational changes upon the binding of CdRP and its conversion to IGP. These findings led us to an extended model that comprises four steps and describes also the kinetic traces of the nonlabeled sIGPS-wt enzyme with high precision. Our data support the significance of the β1α1 and α0α00 loops for substrate binding and catalysis and show that product release is the rate-limiting step of the overall reaction.

dx.doi.org/10.1021/bi301342j | *Biochemistry* 2013, 52, 132−142

MATERIALS AND METHODS

Synthesis of CdRP, rCdRP, and IGP. CdRP was synthesized chemically by incubating anthranilic acid with ribose 5-phosphate[14] and purified by reverse phase high-performance liquid chromatography; rCdRP was synthesized by selective reduction of CdRP with $NaBH_4$.[15] IGP was produced enzymatically from the substrate CdRP using IGPS from *T. maritima*.[16] The enzymes present in the preparation were removed by ultrafiltration.

Site-Directed Mutagenesis. The gene encoding sIGPS, *strp*C, was cloned into the pET21a(+) plasmid (Stratagene) using the restriction sites for *Nhe*I and *Xho*I. Consequently, the recombinant sIGPS protein carries a C-terminal hexahistidine (His_6) tag. Point mutations were introduced into the *strp*C gene by overlap extension polymerase chain reaction (PCR)[17,18] using plasmid pET21a(+)-*strp*C as a template. For the generation of megaprimers by PCR, oligonucleotides T7 terminator (5′-GCTAGTTATTGCTCAGCGG-3′) and 5′-ATTATCTTTATGCAGGCCCTCA-3′ (for construction of *strp*C-R18C) or 5′-TCTGGATTATGTGTTGAAAGG-3′ (for construction of *strp*C-D61C) were used as 5′ primers, and oligonucleotides T7 promotor (5′-TAATACGACTCACTAT-AGGG-3′) and 5′-TGAGGGCCTGCATAAAGATAAT-3′ (for construction of *strp*C-R18C) or 5′-CCTTTCAACACATAAT-CCAGA-3′ (for construction of *strp*C-D61C) were used as 3′-primers (new codons are underlined). The megaprimers were purified and used in a third PCR, together with T7 terminator and T7 promotor primer. The resulting full-length products were digested with *Nhe*I and *Xho*I and ligated into pET21a(+).

Expression and Purification of Recombinant sIGPS. The production of the recombinant sIGPS protein, wild type and Cys variants, was conducted in NEB T7Express Rosetta cells (Stratagene). Cells were grown at 37 °C in LB medium, supplemented with 30 μg/mL chloramphenicol and 150 μg/mL ampicillin. Overexpression was induced when the cells had reached an optical density at 600 nm of 0.6 via addition of IPTG to a final concentration of 1 mM, and growth was continued for 18 h. Purification of all proteins was performed essentially as described previously[13] with minor modifications; e.g., heat precipitation was conducted at 65 °C for 15 min. For the purification of the R18C, D61C, and T186C variants, the dialysis buffer was supplemented with 2 mM DTT to prevent oxidation of cysteines. The purity of the recombinant proteins as judged by sodium dodecyl sulfate−polyacrylamide gel electrophoresis was >95%. Enzyme concentrations were determined by measuring the absorbance at 280 nm, using a molar extinction coefficient of 17210 M^{-1} cm^{-1} as calculated from the amino acid sequence.[19]

Reactivity of Cysteine Residues. Second-order rate constants were determined for the reaction of the sIGPS cysteine variants (R18C, D61C, and T186C) with 5,5′-dithiobis(2-nitrobenzoic acid) (DTNB) using an SX20 stopped-flow instrument (Applied Photophysics). Reaction was initiated by mixing IGPS construct (9.6 μM R18C, 8.1 μM D61C, or 7.7 μM T186C) with DTNB (0.25−1.25 mM) in 20 mM HEPES and 5.0 mM EDTA (pH 7.2) at room temperature (RT). Progress curves were generated by measuring the increase in absorbance of the reaction product TNB^- at 412 nm (ε_{TNB} = 14.15 mM^{-1} cm^{-1}) with time, and the traces were analyzed in a global fit using DynaFit (BioKin Ltd.).[20]

Attachment of Dyes. The sIGPS variants (R18C, D61C, and T186C) were washed with 20 mM HEPES and 5.0 mM EDTA (pH 7.2) to remove DTT. To attach the probes, the variants at concentrations of 50−100 μM and a 1.5-fold excess of the dye [Alexa Fluor 555 (Molecular Probes) or PyMPO (Molecular Probes) in DMSO] were mixed and incubated at RT for 2 h. All steps were performed in the dark to protect the fluorophore. The reaction mixture was washed with 100 mM EPPS containing 10% glycerol (pH 7.5) to remove free dye. Extinction coefficients at 280 nm for each fluorophore in DMSO were determined experimentally using the Nanodrop 2000 instrument (Thermo Scientific) to be 1414.7 μM^{-1} mm^{-1} for Alexa Fluor 555 and 1225.7 μM^{-1} mm^{-1} for PyMPO. To determine the extent of labeling, both the concentrations of the dye and the protein were determined; a 1:1 ratio indicates complete (100%) labeling. The dye concentration was determined by measuring the absorbance of the labeled variants at 412 and 514 nm for PyMPO and Alexa Fluor 555, respectively, and using known extinction coefficients. The protein concentration was determined by measuring the absorbance of the variant at 280 nm, correcting this value by subtracting the contribution of the dye to the absorbance at 280 nm, and using the molar extinction coefficient of sIGPS. The labeled variant was deemed acceptable for use in subsequent experiments if the degree of labeling was >95%. Labeled proteins were stored in 100 mM HEPES buffer (pH 7.5) with 10% glycerol at −80 °C.

Equilibrium Ligand Binding and Steady-State Enzyme Kinetics. Fluorescence titrations were performed at 25 °C in 50 mM EPPS buffer (pH 7.5) and 4.0 mM EDTA using a FluoroMax-4 instrument (Horiba). Aliquots of IGP or rCdRP were added to a solution containing 1.1 μM labeled sIGPS variant and mixed. The complex was equilibrated for 40 s before the signal was monitored. For $R18C^{Alexa555}$ and $D61C^{Alexa555}$, fluorescence emission was measured at 564 nm (10 nm slit) after excitation at 295 nm (1 nm slit) and at 564 nm (4 nm slit) after excitation at 514 nm (1 nm slit), respectively. For $R18C^{PyMPO}$ and $D61C^{PyMPO}$, fluorescence emission was measured at 561 nm (10 nm slit) after excitation at 295 nm (3 nm slit). A minimum of three titrations were performed for the individual ligand−protein pairs. Each of the titrations was corrected by subtracting the average of at least three titrations of protein with buffer (collected under conditions identical to those of the corresponding titrations with the ligands) and fit to the Morrison equation using KaleidaGraph.[21] Steady-state kinetic measurements in 50 mM EPPS buffer (pH 7.5) and 4.0 mM EDTA were performed at 25 °C with a fluorimetric assay as described previously[22,23] using a CARY-Eclipse instrument (Variant). The obtained hyperbolic substrate saturation curves were analyzed with the Michaelis−Menten equation to determine the turnover number (k_{cat}) and the Michaelis constant (K_M^{CdRP}).

Transient Kinetics. Stopped-flow studies were performed at 25 °C in 50 mM EPPS (pH 7.5) and 4 mM EDTA using the SX20 instrument (Applied Photophysics). Tryptophan/IGP fluorescence was excited at 280 nm, and the increase in fluorescence emission was recorded over time using a 335 nm cutoff filter. Single-turnover kinetics of sIGPS were measured by mixing CdRP at a constant concentration (1.0 μM) and protein solutions in a 1:1 volume ratio; the final sIGPS concentration was varied between 1.0 and 15.0 μM. Multiple-turnover kinetics of sIGPS were performed by mixing CdRP at a constant concentration (3.0 μM) with protein solutions in a

1:1 volume ratio; the final sIGPS concentration was varied between 25 and 500 nM. Between five and eight traces were recorded at each protein concentration and averaged.

The change in fluorescence emission intensity of the dye upon ligand binding was recorded over time after mixing labeled sIGPS variants [R18C^{Alexa555}, R18C^{PyMPO}, D61C^{Alexa555}, or D61C^{PyMPO} (0.2 μM)] with IGP or CdRP (2−16 μM) in a 1:1 volume ratio. Emission was recorded with excitation at 295 nm and a 550 nm cutoff filter. Free R18C^{PyMPO} showed a slight increase in the emission intensity upon being mixed with the buffer. To account for this increase, an average of four traces generated in the absence of the ligand was subtracted from progress curves prior to fitting. Single-turnover kinetics of labeled variants were measured by mixing CdRP (2.0 or 4.0 μM) with protein solutions in a 1:1 volume ratio; the final concentration of variants R18C^{Alexa555}, R18C^{PyMPO}, D61C^{Alexa555}, or D61C^{PyMPO} was 12 or 16 μM. Both IGP formation and changes in probe fluorescence were detected for the same solutions.

Data and Global Fitting Analysis. Conventional data fitting of pre-steady-state kinetic data by nonlinear regression using ProData SX and SigmaPlot provided initial estimates for rate constants. The pre-steady-state data from both single-turnover and multiple-turnover experiments with sIGPS-wt were then fit to a single kinetic model by an iterative, global fitting process using DynaFit,[20] which utilizes direct numerical integration to simulate experimental results. With regard to the three-state model, all rate constants (k_1, k_{-1}, k_2, k_3, and k_{-3}) and the associated differential response coefficients (r_{FS}, r_{EP}, and r_P) were optimized in the fit. With regard to the four-state model, the steps in the global fitting procedure are described in Results and the appendant figures. DynaFit also features an error analysis functionality and model discrimination analysis, which was utilized to evaluate the quality of the fit and the degree to which the individual rate constants were constrained by the data.

RESULTS

Steady-State Kinetic Constants. The plasmid-encoded wild-type *trpC* gene from *S. solfataricus* was expressed in *E. coli*, and recombinant sIGPS-wt was purified by heat precipitation of the host proteins followed by metal chelate affinity chromatography. Enzyme kinetic constants of the IGPS reaction were determined at 25 °C using an assay that is based on the increase in fluorescence intensity upon conversion of the substrate CdRP into the product IGP.[7] Consistent with published data,[13,24] the k_{cat} of sIGPS was determined to be 0.062 ± 0.002 s^{-1} and the K_M^{CdRP} to be 51 ± 9 nM, resulting in a k_{cat}/K_M^{CdRP} value of 1.2 × 10^6 M^{-1} s^{-1} (Table 1). Equilibrium fluorescence titration experiments with sIGPS were performed at 25 °C with IGP and the reduced substrate analogue rCdRP (Figure 1A).[15,25] The obtained dissociations (K_d^{rCDRP} = 23 ± 8 nM; K_d^{IGP} = 20 ± 9 nM) testify to an equally high affinity of sIGPS-wt for both ligands. The tight binding of IGP accounts for the product inhibition effect that was observed in multiple-turnover experiments.

Table 1. Steady-State Kinetic Parameters for sIGPS-wt and Cysteine Variants Labeled with Fluorescent Dyes[a]

sIGPS	k_{cat} (s^{-1})	K_M (nM)	k_{cat}/K_M (M^{-1} s^{-1})
wt	0.062 ± 0.002[b]	51 ± 9	1.2 × 10^6
D61C^{Alexa555}	0.038 ± 0.001[b]	46 ± 7	0.83 × 10^6
D61C^{PyMPO}	0.065 ± 0.002[b]	109 ± 11	0.60 × 10^6
R18C^{Alexa555}	0.042 ± 0.001[b]	50 ± 8	0.84 × 10^6
R18C^{PyMPO}	0.040 ± 0.001[b]	45 ± 5	0.89 × 10^6

[a]IGP formation was monitored after mixing of 10 nM enzyme with 0.005−10 μM CdRP. [b]Error in regression.

Stopped-Flow Studies of the sIGPS Reaction. We performed pre-steady-state kinetic measurements with a stopped-flow apparatus to determine the rate constants of the individual steps of the sIGPS reaction. The kinetics of IGP formation under single-turnover conditions was measured after a constant concentration of CdRP had been mixed with a molar excess of sIGPS. The resulting fluorescence traces were biphasic (Figure 2A) and could be fit to a first approximation with the sum of two exponential functions. The obtained rate constant for the first phase, associated with a negative signal amplitude, increased with an increasing enzyme concentration. Conversely, the rate constant for the second phase, 1.96 ± 0.14 s^{-1}, connected to an increase in the fluorescence signal, was identical within error regardless of enzyme concentration. However, the in-depth analysis of the fluorescence traces was complicated by the fact that the intrinsic tryptophan fluorescence of sIGPS-wt, which derives from a single Trp

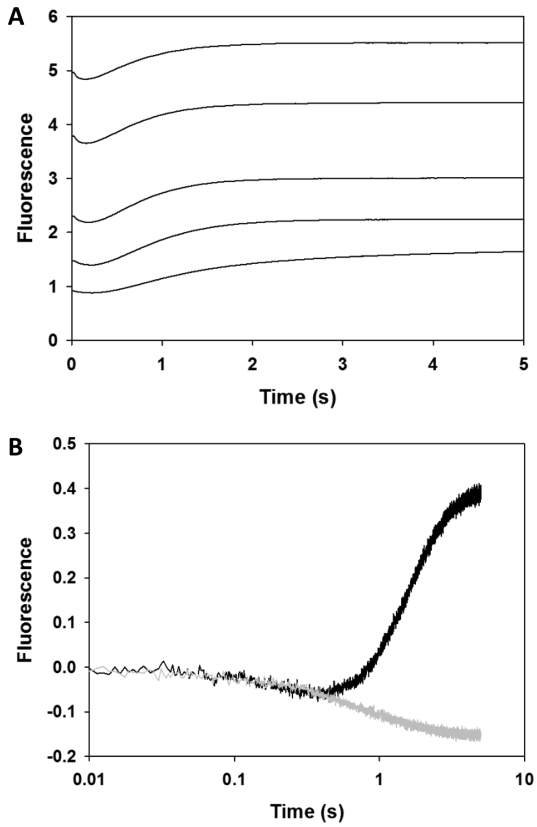

Figure 2. Single-turnover kinetics of the sIGPS-wt reaction. (A) Kinetic traces monitoring Trp/IGP fluorescence (excitation and emission cutoffs of 280 and 335 nm, respectively) were recorded at 25 °C in a stopped-flow apparatus after 1.0 μM CdRP (final concentration) had been mixed with various sIGPS concentrations (final concentrations from botton to top, 1.0, 2.5, 5.0, 10.0, and 15.0 μM, respectively). (B) Overlay of the stopped-flow traces recorded with a 320 nm interference filter during the reaction of 1.0 μM sIGPS with 0.25 μM CdRP (black line) or 0.25 μM rCdRP (gray line) (logarithmic time scale).

dx.doi.org/10.1021/bi301342j | *Biochemistry* 2013, 52, 132−142

residue, Trp8, in the α0 helix (Figure 1B), and the intrinsic IGP fluorescence are highly similar, both showing excitation and emission maxima at 280 and >320 nm, respectively. For this reason, several processes can in principle determine the stopped-flow traces: formation of the enzyme−substrate complex, conversion of CdRP into IGP, and dissociation of the enzyme−product complex.

We compared single-turnover traces of sIGPS-wt in the presence of substrate CdRP with binding kinetics in the presence of its reduced analogue, rCdRP, to discriminate signals accompanying the formation of the enzyme−substrate complex from signals resulting from subsequent processes. With excitation at 280 nm, emission was monitored using a 320 nm interference filter to minimize contributions from the intrinsic fluorescence of rCdRP. A representative overlay of two traces is shown in Figure 2B. The first phase is visible in the presence of both rCdRP and CdRP and is likely to represent the formation of the enzyme−substrate complex. The second phase is seen only when sIGPS reacts with CdRP and is likely associated with formation of the fluorescent product IGP.

Multiple-turnover experiments of the sIGPS reaction were performed by mixing different concentrations of sIGPS with a molar excess of CdRP. The resulting traces showed a pre-steady-state burst of IGP formation followed by a steady state (Figure 3A), which means that IGP formation in the first turnover was faster than in subsequent turnovers. The observed burst rate constant increased with sIGPS-wt concentration in a hyperbolic manner and achieved a maximal value of 0.98 ± 0.03 s^{-1} with a $K_{1/2}$ of 11 ± 2 nM (Figure 3B). The $K_{1/2}$ in this case equals $(k_2 + k_{-1})/k_1$ and is dominated by k_2. The subsequent global fitting analysis indicated that product rebinding and the attendant product inhibition effect are responsible for deviations from linearity in the steady-state phase (Figure S1 of the Supporting Information).

Analysis of IGP Accumulation Data for sIGPS-wt with a Three-State Kinetic Model. The stopped-flow data recorded under single- and multiple-turnover conditions (Figures 2A and 3A) were fit globally to obtain a single set of kinetic parameters. An initial analysis was performed with the three-step mechanism shown in Scheme 1.

Scheme 1

$$E + S \underset{k_{-1}}{\overset{k_1}{\rightleftharpoons}} FS \xrightarrow{k_2} FP \underset{k_{-3}}{\overset{k_3}{\rightleftharpoons}} E + P$$

This mechanism implies that upon binding of CdRP (S) the intrinsic fluorescence of the enzyme (E) changes (to F), chemistry occurs, and IGP (P) is released while the enzyme returns back to the resting fluorescent state (E). The three chemical steps in the proposed IGPS mechanism, condensation, decarboxylation, and dehydration, were merged to one irreversible chemical transformation step described by rate constant k_2. Also, in this initial model, release of product was included as a one-step process. A global analysis with the integrated form of the equation depicted in Scheme 1 using DynaFit[20] yielded values for the individual rate constants, which are summarized in Table 2. The results indicate that the release of product IGP from the active site of sIGPS is the rate-limiting step of the reaction (k_3 = 0.078 s^{-1}). The determined rate constant for the chemical transformation step (k_2 = 1.54 s^{-1}) agrees within the bounds of experimental error with the maximal burst rate of 0.98 s^{-1}. The substrate dissociation rate

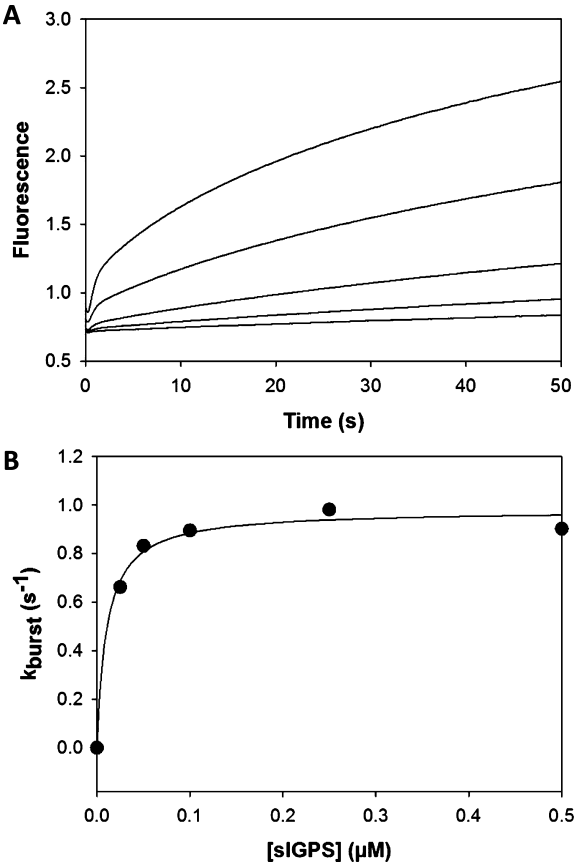

Figure 3. Multiple-turnover kinetics of the sIGPS-wt reaction. (A) Kinetic traces monitoring Trp/IGP fluorescence (excitation and emission cutoffs of 280 and 335 nm, respectively) were recorded at 25 °C in a stopped-flow apparatus after 3.0 μM CdRP (final concentration) had been mixed with various sIGPS concentrations (final concentrations from bottom to top, 25, 50, 100, 250, and 500 nM, respectively). The traces were fit with a burst equation (2−10 s). (B) Plot of the burst rate constant as a function of sIGPS concentration. The data were fit to a hyberbola, yielding a maximal turnover rate constant of 0.98 ± 0.03 s^{-1} with a $K_{1/2}$ of 11 ± 2 nM.

constant could not be accurately resolved; however, an upper limit could be determined (k_{-1} < 0.5 s^{-1}). The three-step mechanism accounts for some key features of the experimental data; nevertheless, significant deviations between stopped-flow transients and the fits (Figure S1 of the Supporting Information) indicate that a more sophisticated analysis is required to satisfactorily explain the data.

Generation of Variants of sIGPS Labeled with Fluorescent Dyes. To detect conformational motions associated with different steps of the enzymatic mechanism of sIGPS, we generated three Cys variants of sIGPS for labeling with fluorescent dyes. The expectation was that structural rearrangements of active site loops during substrate binding or catalysis bring the attached dye into a more hydrophobic or hydrophilic environment, resulting in a change of the emitted fluorescent signal.[26−31] Site-directed mutagenesis was used to introduce cysteines into the N-terminal extension of sIGPS (R18C at the boundary of helix α0 and loop α0α00) or within flexible loops at the catalytic face (D61C in loop β1α1 and T186C in loop β6α6) of the $(\beta\alpha)_8$-barrel[5] (Figure 1B). The mutant genes were expressed in *E. coli*, and the recombinant sIGPS variants were purified as described above for sIGPS-wt. Using DTNB as a model substrate, the three cysteine handles

dx.doi.org/10.1021/bi301342j | *Biochemistry* 2013, 52, 132−142

Table 2. Kinetic Rate Constants for sIGPS-wt Derived from the Global Fit of Single- and Multiple-Turnover Transients to the Three-Step Mechanism Shown in Scheme 1[a]

k_1 (M^{-1} s^{-1})	k_{-1} (s^{-1})	k_2 (s^{-1})	k_3 (s^{-1})	k_{-3} (M^{-1} s^{-1})
$(1.47 \pm 0.02) \times 10^6$	<0.5	1.54 ± 0.06	0.078 ± 0.003	$(6.79 \pm 0.42) \times 10^6$

[a]IGP formation under single-turnover conditions was monitored in stopped-flow experiments by mixing CdRP (1.0 μM) with a molar excess of sIGPS (1.0–15.0 μM). IGP formation under multiple-turnover conditions was monitored under identical conditions by mixing different concentrations of sIGPS (25 nM to 0.5 μM) with a molar excess of CdRP (3.0 μM). An overlay of observed transients with the fit is shown in Figure S1 of the Supporting Information.

were found to have high reactivities, with second-order rate constants of 0.26×10^3, 2.65×10^3, and 3.48×10^3 M^{-1} s^{-1} for the variants R18C, D61C, and T186C, respectively, allowing for fast and efficient labeling with fluorophores Alexa Fluor 555 and PyMPO. The labeled T186C variants exhibited drastically reduced enzymatic activities and were therefore not analyzed any further. In contrast, mutagenesis and labeling of sIGPS at sites 18 and 61 did not significantly alter the steady-state constants of sIGPS (Table 1). Moreover, analysis of rCdRP and IGP binding followed by dye fluorescence revealed only small differences in K_D, k_{on}, and k_{off} for the labeled variants. In addition, K_D values of the labeled variants for rCdRP and IGP equal dissociation constants of sIGPS-wt determined by equilibrium fluorescence titrations (Table 3). Therefore, D61C^{Alexa555}, D61C^{PyMPO}, R18C^{Alexa555}, and R18C^{PyMPO} were deemed good models for sIGPS-wt.

Table 3. Equilibrium and Rate Constants for Binding of IGP and rCdRP to sIGPS Variants Labeled with Fluorescent Dyes[a]

sIGPS	ligand	K_d (nM)	k_{on} (M^{-1} s^{-1})	k_{off} (s^{-1})
wt	IGP	20 ± 9		
wt	rCdRP	23 ± 8		
D61C^{Alexa555}	IGP	29 ± 22	3.47×10^6	0.101
D61C^{Alexa555}	rCdRP	126 ± 23	1.97×10^6	0.236
D61C^{PyMPO}	IGP	28 ± 2.6	1.36×10^6	0.034
D61C^{PyMPO}	rCdRP	32 ± 9.8	0.596×10^6	0.018
R18C^{PyMPO}	IGP	6.4 ± 2.7	6.62×10^6	0.035
R18C^{PyMPO}	rCdRP	143 ± 5.6	3.21×10^6	0.387
R18C^{Alexa555}	IGP	3.6 ± 1.8	10.2×10^6	0.036
R18C^{Alexa555}	rCdRP	92 ± 68	2.8×10^6	0.19

[a]K_D values for sIGPS-wt were determined in fluorescence titration experiments (excitation and emission at 290 and 414 nm, respectively, for rCdRP and 295 and 330 nm, respectively, for IGP). Binding of IGP or rCdRP to sIGPS was monitored in stopped-flow experiments. Values for k_{on} were determined from the linear dependency of k_{on} on ligand concentration. Values of k_{off} were calculated from the relationship $k_{off} = K_d k_{on}$. All k_{on} and k_{off} values were also independently determined using DynaFit, fitting a reversible one-step binding mechanism to the data.

Stopped-Flow Studies of the sIGPS Reaction Catalyzed by Labeled Variants. Pre-steady-state kinetics of IGP formation catalyzed by variants D61C^{Alexa555}, D61C^{PyMPO}, R18C^{Alexa555}, and R18C^{PyMPO} were investigated under single-turnover conditions with a stopped-flow instrument. After CdRP had been mixed with a molar excess of protein, both the kinetics of IGP formation and changes in probe fluorescence were studied. Initially, the three-step model in Scheme 1 was fit to the IGP formation data using DynaFit. All ligand binding and release rates were fixed to the values listed in Table 3 (k_{on} and k_{off} for rCdRP correspond to k_1 and k_{-1}, respectively, for CdRP; k_{on} and k_{off} for IGP correspond to k_{-3} and k_3, respectively). The optimal values for k_2 for this model were found to be 1.43 s^{-1} for variant D61C^{Alexa555}, 1.15 s^{-1} for variant D61C^{PyMPO}, 1.00 s^{-1} for variant R18C^{Alexa555}, and 1.07 s^{-1} for variant R18C^{PyMPO}. These values are similar to the k_2 obtained for sIGPS-wt (1.54 s^{-1}). However, as for sIGPS-wt, the agreement between the data and the fit was unsatisfactory (data not shown).

Stopped-Flow Studies of the rCdRP Binding Mechanism of Labeled Variants. Next, we analyzed changes in dye fluorescence emission signals resulting from substrate binding separately from fluorescence changes occurring upon catalysis. To this end, the nonreactive analogue rCdRP was mixed with the sIGPS variants in the stopped-flow apparatus under the same conditions that were used in the IGP formation experiments (enzyme in excess over ligand). Initially, a one-step reversible binding mechanism (Scheme 2) was evaluated for the fluorescence traces.

Scheme 2

$$E + S \underset{k_{-1}}{\overset{k_1}{\rightleftharpoons}} ES$$

The binding and dissociation rate constants for rCdRP (k_1 and k_{-1}, respectively) were again fixed to the values for k_{on} and k_{off}, respectively, listed in Table 3. Analysis using DynaFit showed that this mechanism did not accurately describe the binding traces obtained via probe fluorescence (Figure 4A), which prompted us to explore alternative binding mechanisms. The model shown in Scheme 3 includes a pre-equilibrium between two forms of rCdRP described by k_{-c} and k_c, which could reflect keto–enol tautomerization of CdRP. The model shown in Scheme 4 comprises a conformational change (k_{conf}) that follows the initial binding.

When each model was fit to the data, k_1 and k_{-1} were again fixed to values for k_{on} and k_{off}, respectively, listed in Table 3. Model discrimination analysis revealed that the binding mechanism in Scheme 4 was superior compared to those shown in Schemes 2 and 3 for all four variants. This is illustrated by representative data for the binding of rCdRP to D61C^{Alexa555} in Figure 4. The values of k_{conf} obtained from the best fit to Scheme 4 are listed in Table 4. The small signal amplitude of the probe fluorescence signal for variant R18C^{PyMPO} resulted in a relatively large uncertainty for k_{conf} of this variant.

Analysis of IGP Accumulation Data for Labeled sIGPS Variants with a Four-State Kinetic Model. The conformational change following substrate binding revealed by experiments using rCdRP was incorporated into the three-step model shown in Scheme 1 to give the four-step model shown in Scheme 5.

This model was then fit to the IGP accumulation data that had been obtained under single-turnover conditions. In the fit,

dx.doi.org/10.1021/bi301342j | Biochemistry 2013, 52, 132–142

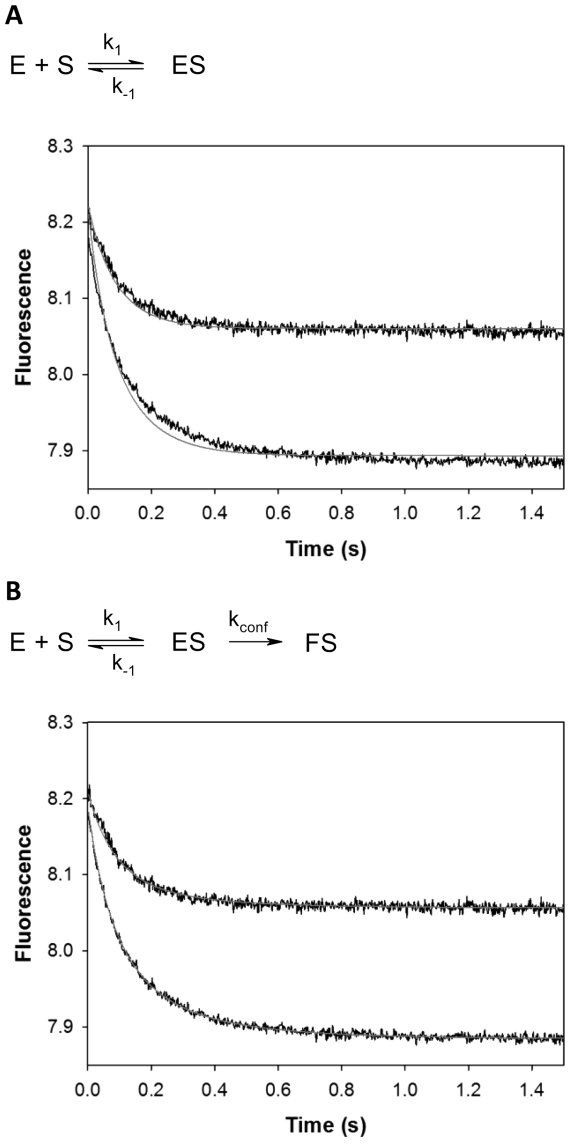

Figure 4. Analysis of the binding reaction of rCdRP with sIGPS-D61C^{Alexa555}. Kinetic traces monitoring Alexa Fluor 555 fluorescence (excitation and emission cutoffs of 514 and 550 nm, respectively) were recorded in a stopped-flow apparatus at 25 °C after 6 μM D61C^{Alexa555} had been mixed with 1 μM rCdRP (top) or 2 μM rCdRP (bottom). A one-step binding model corresponding to Scheme 2 (A) or a two-step binding model corresponding to Scheme 4 (B), where the enzyme undergoes a conformational change after the binding event, was fit to the stopped-flow transients (gray lines). The quality of the fit was significantly better in panel B.

Scheme 3

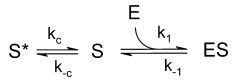

Scheme 4

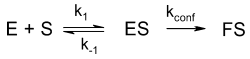

the binding rate constants, k_1, k_{-1}, k_3, and k_{-3}, were again fixed to the values listed in Table 3 (k_{on} and k_{off} for rCdRP correspond to k_1 and k_{-1}, respectively, for CdRP; k_{on} and k_{off} for IGP correspond to k_{-3} and k_3, respectively), and k_{conf} was fixed to the values listed in Table 4. Moreover, the k_2 values obtained from fitting data to the three-step model (Scheme 1) were used as initial guesses. For all four variants, the fit of the four-state mechanism of Scheme 5 to the data is satisfactory (representative data shown for the D61C^{Alexa555} construct in Figure 5) and matches the data much better than the fit with the three-step mechanism of Scheme 1. The optimal k_2 values obtained from the analysis with the four-state model are listed in Table 5.

Table 4. Values of Rate Constant k_{conf} Derived from the Fit According to Scheme 4 of Dye Fluorescence Signals Observed during the Binding of rCdRP to sIGPS Variants[a]

	D61C^{Alexa555}	D61C^{PyMPO}	R18C^{Alexa555}	R18C^{PyMPO}
k_{conf} (s^{-1})	3.39 ± 0.17	0.44 ± 0.031	6.18 ± 0.23	5.63 ± 1.1

[a]Binding of rCdRP to fluorescently labeled sIGPS variants was monitored in stopped-flow experiments by mixing an excess of sIGPS (6 μM) with rCdRP (1 or 2 μM) and monitoring dye fluorescence. In the global fit, rate constants k_1 and k_{-1} were fixed to the values listed in Table 3 (k_1 and k_{-1} equal k_{on} and k_{off}, respectively, in Table 3). Rate constant k_{conf} and response coefficients were optimized.

Scheme 5

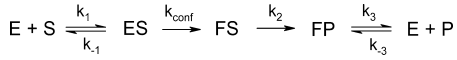

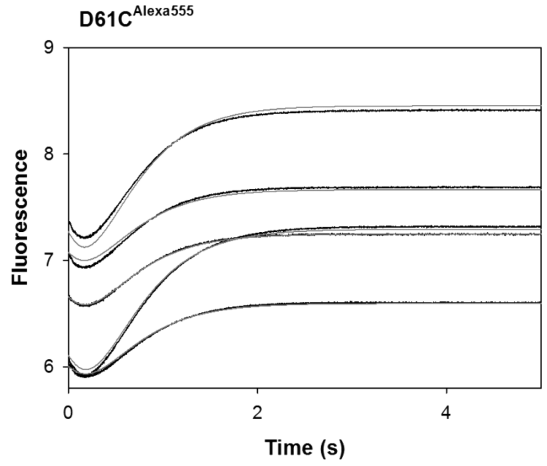

Figure 5. Analysis of single-turnover kinetics of D61C^{Alexa555} using IGP/Trp fluorescence according to Scheme 5. Kinetic fluorescence traces (excitation and emission cutoffs of 280 and 335 nm, respectively) were recorded at 25 °C in a stopped-flow apparatus after 1.0 or 2.0 μM CdRP had been mixed with 6.0, 7.0, or 8.0 μM D61C^{Alexa555} (final concentrations). In the fit, rate constants k_1, k_{-1}, k_3, k_{-3}, and k_{conf} were fixed to the values listed in Table 3 (k_{on} and k_{off} for rCdRP correspond to k_1 and k_{-1}, respectively, for CdRP; k_{on} and k_{off} for IGP correspond to k_{-3} and k_3, respectively) and Table 4, and k_2 and response coefficients were optimized in the fit. Black lines show the data and gray lines the fit.The global fit parameters for all four labeled sIGPS variants are summarized in Table 5.

Analysis of Dye Fluorescence Data for Labeled sIGPS Variants with the Four-State Kinetic Model. Next, single-turnover experiments in which dye fluorescence was followed instead of IGP accumulation were performed. The direction of change in dye fluorescence was different for the Alexa and PyMPO probes. The transients associated with variants

dx.doi.org/10.1021/bi301342j | Biochemistry 2013, 52, 132−142

Table 5. Kinetic Rate Constants for Fluorescently Labeled sIGPS Variants Derived from the Global Fit of the Single-Turnover Transients to the Mechanism Shown in Scheme 5[a]

	D61C^{Alexa555}	D61C^{PyMPO}	R18C^{Alexa555}	R18C^{PyMPO}
k_1 (M^{-1} s^{-1})	1.97×10^6	0.60×10^6	2.80×10^6	3.21×10^6
k_{-1} (s^{-1})	0.24	0.018	0.19	0.39
k_{conf} (s^{-1})	3.39	0.44	6.18	5.63
k_2 (s^{-1})	2.47 ± 0.014	1.27 ± 0.0032	1.35 ± 0.0022	1.49 ± 0.0034
k_3 (s^{-1})	0.101	0.034	0.036	0.035
k_{-3} (M^{-1} s^{-1})	3.47×10^6	1.36×10^6	10.2×10^6	6.62×10^6

[a]IGP formation under single-turnover conditions was monitored in stopped-flow experiments by mixing CdRP (1.0 or 2.0 μM) with a molar excess of the labeled sIGPS variants (6.0, 7.0, or 8.0 μM). Ligand binding constants k_1, k_{-1}, k_3, and k_{-3} were fixed to values listed in Table 3, and the k_{conf} values were fixed to the values listed in Table 4. The best fit k_2 values that are consistent with all data are given here.

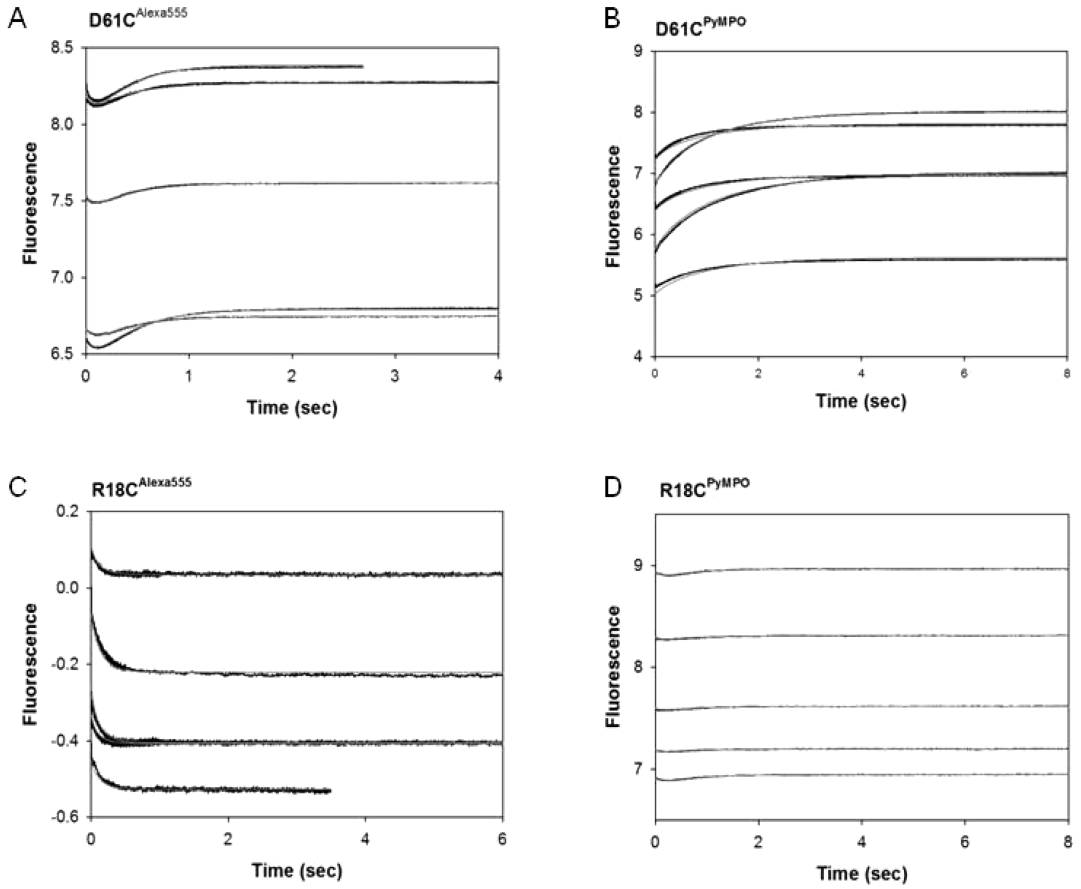

Figure 6. Analysis of single-turnover kinetics of labeled sIGPS variants using dye fluorescence according to Scheme 5. Kinetic fluorescence traces (excitation and emission cutoffs of 412 and 550 nm, respectively, for PyMPO and 514 and 550 nm, respectively, for Alexa Fluor 555) were recorded at 25 °C in a stopped-flow apparatus after 1.0 or 2.0 μM CdRP had been mixed with 6.0, 7.0, or 8.0 μM labeled sIGPS variant (final concentration). The extended mechanism shown in Scheme 5 (D61C^{Alexa555}, D61C^{PyMPO}, and R18C^{PyMPO}) or the binding mechanism in Scheme 4 (R18C^{Alexa555}) was fit to the transients. In the fit, the rate constants were fixed to the values listed in Table 5, and response coefficients were optimized. The black lines show the data and the gray lines the fit.

D61C^{Alexa555} and R18C^{PyMPO} showed biphasic behavior with negative signal amplitude for the first phase and small positive signal amplitude for the second (Figure 6A,D). Variant R18C^{Alexa555} depicts transients with a decrease in dye fluorescence (Figure 6C), while variant D61C^{PyMPO} transients show an increase in fluorescence (Figure 6B). The four-state kinetic model was used to describe the dye fluorescence data by applying the rate constants obtained from analysis of the IGP accumulation data (Table 5). The response coefficients were optimized for each labeled sIGPS variant separately. For variants D61C^{Alexa555} and D61C^{PyMPO}, the four-state model allowed for a good fit of the data (Figure 6A,B), which means that the dyes in loop $\beta1\alpha1$ are sensitive to both the conformational switch following substrate binding and the chemical step of IGP formation. For variant R18C^{Alexa555}, only a binding event followed by a conformational change was detected by following probe fluorescence, whereas no signal change was associated with the chemistry step (Figure 6C). The model in Scheme 4 was successfully fit to these transients. This finding is consistent with involvement of helix $\alpha0$ (on which residue 18 is located) in binding but not in the chemistry step of IGP catalysis. As in the rCdRP binding experiments discussed above, the dye fluorescence traces associated with R18C^{PyMPO} (Figure 6D) had very small amplitudes that could

dx.doi.org/10.1021/bi301342j | *Biochemistry* 2013, 52, 132−142

be fit to many different rate constants and thus did not result in a conclusive result. However, also for this variant, the four-state model provides a much better fit to the data than the three-step mechanism. Variants R18C^{PyMPO}, R18C^{Alexa555}, and D61C^{Alexa555} have relatively similar k_1 and k_{conf} values (Table 5). However, for the D61C^{PyMPO} variant, both k_1 and k_{conf} are significantly reduced compared to those of the other variants, for unknown reasons.

Analysis of IGP Accumulation Data for sIGPS-wt with the Four-State Kinetic Model. Pre-steady-state measurements with the fluorescently labeled sIGPS-D61C and -R18C variants were best fit with the mechanism shown in Scheme 5 in which a conformational change follows ligand binding. We assessed whether inclusion of this conformation change would also improve the quality of the fit when analyzing the single-turnover measurements that were performed with sIGPS-wt. Indeed, inclusion of k_{conf} did improve the fit to the turnover data of sIGPS-wt significantly (Figure S2 of the Supporting Information) compared to the fit with the three-state mechanism (Figure S1 of the Supporting Information). Model discrimination analysis[32] shown in the Supporting Information confirmed that the binding mechanism shown in Scheme 5 was superior compared to the simpler mechanism in Scheme 1, indicating that the improved quality of the fit is not due to an artifact caused by an increased number of optimized parameters. The values obtained for microscopic rate constants k_1, k_{-1}, k_{conf}, k_2, k_3, and k_{-3} are close to the parameters obtained for the fluorescently labeled sIGPS variants listed in Table 5. The rate of conformational change (k_{conf} = 5.69 s^{-1}) is fast in comparison to the dissociation rate of the enzyme−substrate complex (k_{-1} < 0.1 s^{-1}), so that substrate in the initial encounter complex is bound to be turned over. Moreover, the rate of chemical transformation (k_2 = 1.54 s^{-1}) is much faster than the rate of product release (k_{-3} = 0.078 s^{-1}), which is the rate-limiting step of the catalytic mechanism.

Using the fluorescently labeled D61C and R18C variants, we were able to extract additional information about the loop motions that accompany binding and chemistry. This information about conformational motions would not have been accessible if we had monitored the intrinsic Trp fluorescence and fluorescence of the nascent product IGP alone. With the combination of product fluorescence and emission of exogenously added fluorescence tags, we now have established methods and probes for relating structure, loop motions, and kinetics.

DISCUSSION

Stopped-flow single- and multiple-turnover transients of sIGPS-wt were first analyzed with a minimal kinetic reaction mechanism, which comprises three steps: reversible substrate binding (k_1 and k_{-1}), irreversible chemical transformation (k_2), and reversible product release (k_3 and k_{-3}) (Scheme 1). Although this analysis unambiguously showed that the chemical transformation step is fast and that the rate of the overall reaction at 25 °C is limited by product release, the three-state model did not describe the data in a satisfactory manner. The comparison of crystal structures of sIGPS with bound substrate (analogue) and product as well as MD simulations suggested that the binding of CdRP and its on-enzyme conversion to IGP goes along with conformational transitions at the catalytic face of the $(\beta\alpha)_8$-barrel.[11−13] We used sIGPS variants covalently labeled with fluorescent dyes at position 18 in helix α0 of the N-terminal extension and at residue 61 in flexible loop $\beta1\alpha1$ to visualize such conformational motions and to refine our kinetic mechanism. The time-dependent analysis of dye fluorescence after rCdRP had been mixed with the labeled variants revealed a conformational change that follows substrate binding, which led us to formulate an extended four-step kinetic model (Scheme 5). This model satisfactorily describes the single-turnover IGP accumulation data of both labeled variants (Figure 5) and sIGPS-wt (Figure S2 of the Supporting Information).

Importantly, when the same single-turnover data were analyzed using the probe fluorescence instead of the product formation signal, the results differed depending on the position of the fluorophore. Dyes attached to position 18 of helix α0 predominantly reported on the substrate-induced conformational switch. Specifically, for R18C^{Alexa555}, there is no change in probe fluorescence emission associated with the chemistry step, and for R18C^{PyMPO}, the signal amplitude is very small. These findings are consistent with the role of the N-terminal extension of sIGPS in substrate binding, rather than in chemistry. In accordance with this conclusion, N-terminally truncated variants of sIGPS display unchanged turnover numbers but Michaelis constants for CdRP that are increased by 3 orders of magnitude in comparison to that of sIGPS-wt.[13] In contrast, dyes attached to position 61 reported on both the substrate-induced conformational switch and the chemistry step. The probes at position 61 are located on the same $\beta1\alpha1$ loop as Lys53, which positions reactive atoms C1 and C2′ of CdRP and is thought to guide the substrate and the reaction intermediates from one active site pocket to another upon generation of IGP. This guiding function of Lys53 will require conformational flexibility of loop $\beta1\alpha1$,[11] which was likely monitored by the dyes attached to residue 61. The important role of the $\beta1\alpha1$ loop for catalysis identified in our study is in line with previous findings that it constitutes an activity "hot spot". A combination of random mutagenesis and metabolic selection identified 18 single activating substitutions leading to an increased turnover number of sIGPS. Six of those 18 exchanges were located at different positions within loop $\beta1\alpha1$, although it comprises only ∼5% of the amino acids of sIGPS.[24]

In our kinetic models, the three chemical steps in the IGPS mechanism, condensation, decarboxylation, and dehydration, were merged to one irreversible chemical transformation step described by rate constant k_2. Interestingly, there was no kinetic evidence of the two intermediates, very likely because the fluorescence capacities of the intermediates under the applied experimental conditions were similar. Basso and co-workers studied the kinetics of the mtIGPS reaction using electrospray ionization mass spectrometry and were able to trap two intermediates for this homologue,[33] providing indirect support for the existence of the two intermediates.

Studies of the solvent viscosity effect by Boehr and co-workers indicate that the identity of the rate-limiting step of sIGPS changes with temperature.[34] Whereas product release is rate-determining at 25 °C, a proton transfer step succeeding CO_2 release becomes the slowest step of the overall reaction at the physiologically relevant temperature of 75 °C. The active sites of IGPS enzymes are well-shielded from solvent, and thus, product release must be accompanied by conformational changes. These conformational changes may limit the rate of product release at lower temperatures, while their motion may be accelerated at higher temperatures, making product release faster and no longer rate-determining. Also, the chemical step of the reaction is proposed to accelerate with temperature

dx.doi.org/10.1021/bi301342j | Biochemistry 2013, 52, 132−142

because of an increased flexibility of the Lys53 side chain.[11,12] In the future, it will be interesting to examine the temperature dependence of ssIGPS using fluorescent tags and stopped-flow methods. Substrate binding was shown to be a two-step process (Scheme 5). It is therefore plausible that product release might also comprise two steps, a conformational rearrangement followed by product dissociation. However, in stopped-flow experiments monitoring dye fluorescence during the binding of IGP to the labeled sIGPS variants, a one-step process is observed (Table 3). The rate constants obtained in the binding experiments are valid when single-turnover data of the labeled sIGPS variants are being described (Table 5). In addition, global analysis of the multiple-turnover experiments with sIGPS-wt yields very similar product association and dissociation rates (k_3 and k_{-3}, respectively, in Table 1), and inclusion of a two-step product dissociation does not improve the quality of the fit. These observations indicate that loop motion and product dissociation proceed in a concerted manner with similar rates and cannot be distinguished with the applied fluorescence probes. At this point, we cannot decide whether loop movement itself or dissociation of the product limits the rate of product release.

An example in which a slow product release step has been shown to relate to movement of a solvent-exposed loop is the OMP synthase from *Salmonella typhimurium*.[35,36] In this dimeric enzyme with a Rossmann-type nucleotide binding fold, the movement of a flexible loop appears to be integral to catalysis, both to cover the active site and to recruit essential residues to the catalytic locus. NMR studies revealed that loop opening and product release make up a two-step process, the overall rate of which is partially rate-limiting. Another very-well characterized enzyme for which rate-limiting product release is associated with conformational changes in loops is triosephosphate isomerase (TIM),[37] which adopts a $(\beta\alpha)_8$-barrel fold similar to that of sIGPS. It has been shown that substrate and product binding are multistep processes in which the very fast formation of the enzyme substrate encounter complex is followed by a slower unimolecular loop closure conformational switch. Elegant solid-state NMR studies show that the loop opening−closing mechanism is not ligand-gated, but an intrinsic property of both the nonliganded and the liganded state.[38] Both OMP synthase and TIM have in common the fact that substrate and product binding employ similar conformational motions; this seems to be a difference with respect to sIGPS. However, a more detailed analysis of conformational dynamics associated with product release using NMR methods is necessary to clarify this notion.

■ ASSOCIATED CONTENT

Supporting Information

Analysis of reaction kinetics of sIGPS-wt according to Scheme 1 (Figure S1), analysis of reaction kinetics of sIGPS-wt according to Scheme 5 (Figure S2), model discrimination analysis (Tables S1 and S2), and a supporting reference. This material is available free of charge via the Internet at http://pubs.acs.org.

■ AUTHOR INFORMATION

Corresponding Author

*S.S.: phone, +49-941-943 3339; fax, +49-941-943 2813; e-mail, sandra.schlee@biologie.uni-regensburg.de. N.M.G.: phone, (973) 655-3410; fax, (973) 655-7772; e-mail, goodeyn@mail.montclair.edu.

Funding

We are thankful for the National Science Foundation Graduate STEM Fellows in K-12 Education (GK-12) Program (Grant 0638708).

Notes

The authors declare no competing financial interest.

■ ACKNOWLEDGMENTS

We sincerely thank Professor Stephen J. Benkovic for his guidance and vision throughout this project. We thank Sonja Fuchs, Rita C. McDonough, Ruqaiya Naqvi, and Alexandra Zumba for expert technical assistance and Dietmar Birzer for help with the generation of figures.

■ ABBREVIATIONS

CdRP, 1-(*o*-carboxyphenylamino)-1-deoxyribulose 5-phosphate; rCdRP, reduced CdRP; IGP, indole-3-glycerol phosphate; IGPS, IGP synthase; sIGPS, IGPS from *S. solfataricus*; DTT, dithiothreitol; DTNB, 5,5′-dithiobis(2-nitrobenzoic acid).

■ REFERENCES

(1) Parry, R. J. (1972) Biosynthesis of compounds containing an indole nucleus. In *The Chemistry of Heterocyclic Compounds in Indoles*, pp 1−64, Wiley-Interscience, New York.

(2) Wilmanns, M., Priestle, J. P., Niermann, T., and Jansonius, J. N. (1992) Three-dimensional structure of the bifunctional enzyme phosphoribosylanthranilate isomerase: Indoleglycerolphosphate synthase from *Escherichia coli* refined at 2.0 Å resolution. *J. Mol. Biol. 223*, 477−507.

(3) Priestle, J. P., Grutter, M. G., White, J. L., Vincent, M. G., Kania, M., Wilson, E., Jardetzky, T. S., Kirschner, K., and Jansonius, J. N. (1987) Three-dimensional structure of the bifunctional enzyme N-(5′-phosphoribosyl)anthranilate isomerase-indole-3-glycerol-phosphate synthase from *Escherichia coli*. *Proc. Natl. Acad. Sci. U.S.A. 84*, 5690−5694.

(4) Knochel, T. R., Hennig, M., Merz, A., Darimont, B., Kirschner, K., and Jansonius, J. N. (1996) The crystal structure of indole-3-glycerol phosphate synthase from the hyperthermophilic archaeon *Sulfolobus solfataricus* in three different crystal forms: Effects of ionic strength. *J. Mol. Biol. 262*, 502−515.

(5) Hennig, M., Darimont, B., Sterner, R., Kirschner, K., and Jansonius, J. N. (1995) 2.0 Å structure of indole-3-glycerol phosphate synthase from the hyperthermophile *Sulfolobus solfataricus*: Possible determinants of protein stability. *Structure 3*, 1295−1306.

(6) Knochel, T., Pappenberger, A., Jansonius, J. N., and Kirschner, K. (2002) The crystal structure of indoleglycerol-phosphate synthase from *Thermotoga maritima*. Kinetic stabilization by salt bridges. *J. Biol. Chem. 277*, 8626−8634.

(7) Darimont, B., Stehlin, C., Szadkowski, H., and Kirschner, K. (1998) Mutational analysis of the active site of indoleglycerol phosphate synthase from *Escherichia coli*. *Protein Sci. 7*, 1221−1232.

(8) Eberhard, M., and Kirschner, K. (1989) Modification of a catalytically important residue of indoleglycerol-phosphate synthase from *Escherichia coli*. *FEBS Lett. 245*, 219−222.

(9) Hennig, M., Darimont, B. D., Jansonius, J. N., and Kirschner, K. (2002) The catalytic mechanism of indole-3-glycerol phosphate synthase: crystal structures of complexes of the enzyme from *Sulfolobus solfataricus* with substrate analogue, substrate, and product. *J. Mol. Biol. 319*, 757−766.

(10) Mazumder-Shivakumar, D., and Bruice, T. C. (2004) Molecular dynamics studies of ground state and intermediate of the hyperthermophilic indole-3-glycerol phosphate synthase. *Proc. Natl. Acad. Sci. U.S.A. 101*, 14379−14384.

(11) Mazumder-Shivakumar, D., Kahn, K., and Bruice, T. C. (2004) Computational study of the ground state of thermophilic indole

glycerol phosphate synthase: Structural alterations at the active site with temperature. *J. Am. Chem. Soc. 126*, 5936−5937.
(12) Bruice, T. C. (2006) Computational approaches: Reaction trajectories, structures, and atomic motions. Enzyme reactions and proficiency. *Chem. Rev. 106*, 3119−3139.
(13) Schneider, B., Knochel, T., Darimont, B., Hennig, M., Dietrich, S., Babinger, K., Kirschner, K., and Sterner, R. (2005) Role of the N-terminal extension of the $(\beta\alpha)_8$-barrel enzyme indole-3-glycerol phosphate synthase for its fold, stability, and catalytic activity. *Biochemistry 44*, 16405−16412.
(14) Creighton, T. E., and Yanofsky, C. (1970) Chorismate to tryptophan (*Escherichia coli*): Anthranilate synthetase, PR transferase, PRA isomerase, InGP synthetase, tryptophan synthetase. *Methods Enzymol. 17A*, 365−380.
(15) Bisswanger, H., Kirschner, K., Cohn, W., Hager, V., and Hansson, E. (1979) N-(5-Phosphoribosyl)anthranilate isomerase-indoleglycerol-phosphate synthase. 1. A substrate analogue binds to two different binding sites on the bifunctional enzyme from *Escherichia coli*. *Biochemistry 18*, 5946−5953.
(16) Merz, A., Knochel, T., Jansonius, J. N., and Kirschner, K. (1999) The hyperthermostable indoleglycerol phosphate synthase from *Thermotoga maritima* is destabilized by mutational disruption of two solvent-exposed salt bridges. *J. Mol. Biol. 288*, 753−763.
(17) Horton, R. M., Hunt, H. D., Ho, S. N., Pullen, J. K., and Pease, L. R. (1989) Engineering hybrid genes without the use of restriction enzymes: Gene splicing by overlap extension. *Gene 77*, 61−68.
(18) Ho, S. N., Hunt, H. D., Horton, R. M., Pullen, J. K., and Pease, L. R. (1989) Site-directed mutagenesis by overlap extension using the polymerase chain reaction. *Gene 77*, 51−59.
(19) Pace, C. N., Vajdos, F., Fee, L., Grimsley, G., and Gray, T. (1995) How to measure and predict the molar absorption coefficient of a protein. *Protein Sci. 4*, 2411−2423.
(20) Kuzmic, P. (1996) Program DYNAFIT for the analysis of enzyme kinetic data: application to HIV proteinase. *Anal. Biochem. 237*, 260−273.
(21) Morrison, J. F. (1969) Kinetics of the reversible inhibition of enzyme-catalysed reactions by tight-binding inhibitors. *Biochim. Biophys. Acta 185*, 269−286.
(22) Eberhard, M., Tsai-Pflugfelder, M., Bolewska, K., Hommel, U., and Kirschner, K. (1995) Indoleglycerol phosphate synthase-phosphoribosyl anthranilate isomerase: Comparison of the bifunctional enzyme from *Escherichia coli* with engineered monofunctional domains. *Biochemistry 34*, 5419−5428.
(23) Hommel, U., Eberhard, M., and Kirschner, K. (1995) Phosphoribosyl anthranilate isomerase catalyzes a reversible Amadori reaction. *Biochemistry 34*, 5429−5439.
(24) Merz, A., Yee, M. C., Szadkowski, H., Pappenberger, G., Crameri, A., Stemmer, W. P., Yanofsky, C., and Kirschner, K. (2000) Improving the catalytic activity of a thermophilic enzyme at low temperatures. *Biochemistry 39*, 880−889.
(25) Henn-Sax, M., Thoma, R., Schmidt, S., Hennig, M., Kirschner, K., and Sterner, R. (2002) Two $(\beta\alpha)_8$-barrel enzymes of histidine and tryptophan biosynthesis have similar reaction mechanisms and common strategies for protecting their labile substrates. *Biochemistry 41*, 12032−12042.
(26) Boyd, A. E., Dunlop, C. S., Wong, L., Radic, Z., Taylor, P., and Johnson, D. A. (2004) Nanosecond dynamics of acetylcholinesterase near the active center gorge. *J. Biol. Chem. 279*, 26612−26618.
(27) Desamero, R., Rozovsky, S., Zhadin, N., McDermott, A., and Callender, R. (2003) Active site loop motion in triosephosphate isomerase: T-jump relaxation spectroscopy of thermal activation. *Biochemistry 42*, 2941−2951.
(28) Tsai, Y. C., and Johnson, K. A. (2006) A new paradigm for DNA polymerase specificity. *Biochemistry 45*, 9675−9687.
(29) Tsai, Y. C., Jin, Z., and Johnson, K. A. (2009) Site-specific labeling of T7 DNA polymerase with a conformationally sensitive fluorophore and its use in detecting single-nucleotide polymorphisms. *Anal. Biochem. 384*, 136−144.
(30) Goodey, N. M., Alapa, M. T., Hagmann, D. F., Korunow, S. G., Mauro, A. K., Kwon, K. S., and Hall, S. M. (2011) Development of a fluorescently labeled thermostable DHFR for studying conformational changes associated with inhibitor binding. *Biochem. Biophys. Res. Commun. 413*, 442−447.
(31) Antikainen, N. M., Smiley, R. D., Benkovic, S. J., and Hammes, G. G. (2005) Conformation coupled enzyme catalysis: Single-molecule and transient kinetics investigation of dihydrofolate reductase. *Biochemistry 44*, 16835−16843.
(32) Burnham, K. P., and Anderson, D. R. (2002) *Model selection and multimodel inference: A practical information-theoretic approach*, 2nd ed., Springer Science+Business Media, Inc.
(33) Czekster, C. M., Neto, B. A., Lapis, A. A., Dupont, J., Santos, D. S., and Basso, L. A. (2009) Steady-state kinetics of indole-3-glycerol phosphate synthase from *Mycobacterium tuberculosis*. *Arch. Biochem. Biophys. 486*, 19−26.
(34) Zaccardi, M. J., Mannweiler, O., and Boehr, D. D. (2012) Differences in the catalytic mechanisms of mesophilic and thermophilic indole-3-glycerol phosphate synthase enzymes at their adaptive temperatures. *Biochem. Biophys. Res. Commun. 418*, 324−329.
(35) Wang, G. P., Cahill, S. M., Liu, X., Girvin, M. E., and Grubmeyer, C. (1999) Motional dynamics of the catalytic loop in OMP synthase. *Biochemistry 38*, 284−295.
(36) Wang, G. P., Lundegaard, C., Jensen, K. F., and Grubmeyer, C. (1999) Kinetic mechanism of OMP synthase: A slow physical step following group transfer limits catalytic rate. *Biochemistry 38*, 275−283.
(37) Wierenga, R. K., Kapetaniou, E. G., and Venkatesan, R. (2010) Triosephosphate isomerase: A highly evolved biocatalyst. *Cell. Mol. Life Sci. 67*, 3961−3982.
(38) Williams, J. C., and McDermott, A. E. (1995) Dynamics of the flexible loop of triosephosphate isomerase: The loop motion is not ligand gated. *Biochemistry 34*, 8309−8319.